

Soft-x-ray magnetic speckles from a nanostructured FePd wireK. Chesnel,^{1,*} M. Belakhovsky,¹ F. Livet,^{2,†} S. P. Collins,³ G. van der Laan,^{3,‡} S. S. Dhesi,⁴ J. P. Attané,¹ and A. Marty¹¹CEA Grenoble, Département de Recherche Fondamentale sur la Matière Condensée, Service de Physique des Matériaux et Microstructures, 17, Rue des Martyrs, F-38054 Grenoble Cedex 9, France²LTPCM / INPG GRENOBLE, ENSEEG-Domaine Universitaire, BP 75-38402 Saint-Martin d'Hères Cedex, France³Magnetic Spectroscopy Group, Daresbury Laboratory, Warrington WA4 4AD, United Kingdom⁴ESRF, BP 220, 38054 Grenoble, France

(Received 21 August 2002; published 11 November 2002)

We have recorded magnetic speckle patterns of unprecedented quality on a tiny sample using soft-x-ray resonant magnetic scattering in reflection geometry. This geometry is well suited to the study of epitaxial thin films. The microscopic object consisted of an FePd wire with transversal stripe domains of alternatingly up and down magnetization. Sharp magnetic superstructure peaks reflect the domain periodicity, whereas the magnetic speckles give access to the domain morphology. A high degree of coherence has been obtained ($\beta=0.85$) as evidenced from the strong observed intensity fluctuations.

DOI: 10.1103/PhysRevB.66.172404

PACS number(s): 75.75.+a, 75.25.+z, 75.70.-i

Patterned magnetic media are currently under extensive study, since they offer great potential to overcome the superparamagnetic limit for storage devices. A crucial aim is to understand the magnetic interactions with varying size and density of the individual nanostructured objects. At present, several spatial-resolving techniques are available to study magnetic nanostructures, but soft-x-ray resonant magnetic scattering (SXRMS) is one of the most versatile since it can be used in a magnetic field and is element specific, with a high potential for spatial and temporal resolution.¹⁻³ Transition metals and rare earths have strong magneto-optical resonances in the soft-x-ray range, making SXRMS ideal to study magnetic interactions in patterned media. In addition, for soft x rays the available coherent flux is expected to be two orders of magnitude larger than for comparable experiments in the hard-x-ray region.⁴ To date, many coherent x-ray studies have concentrated on structural disorder using intensity-fluctuation spectroscopy. The evolution of the diffraction pattern is monitored as a function of time or temperature, giving access to dynamical processes.⁴⁻⁷ Very few studies have been done in the soft-x-ray region and mainly in transmission geometry which severely limits the general applicability due to the very thin substrates need.^{8,9} In this paper, we report magnetic speckles in coherent SXRMS in reflection geometry from an isolated microscopic FePd wire. The results obtained on the wire demonstrate the feasibility of coherent SXRMS for individual patterned microstructures.

FePd thin-film alloys provide an ideal means for demonstrating the potential of soft-x-ray magnetic speckle imaging. These films are grown on a MgO substrate using molecular beam epitaxy¹⁰ and exhibit a perpendicular magnetocrystalline anisotropy.¹¹ The competition between dipolar and magnetic anisotropy leads to a stripe configuration with alternating domains of up and down magnetization as shown on the magnetic force microscopy (MFM) image in Fig. 1. The stripe domains are well ordered along the direction of a magnetic field applied after the growth process and have a width of ~ 50 nm, giving a magnetic periodicity of ~ 100 nm. The MFM image reveals the presence of various types of defects, such as domain wall meandering and forks. In SXRMS, imaging is performed in reciprocal space with the objective of

reconstructing the diffraction pattern into a real-space representation of the magnetic structure. Complementarity between the two techniques can be expected, but SXMRM, apart from being element specific, is also a vector magnetometer with a high degree of lateral and depth sensitivity. For magnetic speckle imaging, transversely coherent photons must be selected from the incident beam. This can be achieved by inserting a pinhole in the beam, close to the sample, or by using a microscopic sample of a size comparable to the transverse coherence length. The second approach would have the advantage that it allows a comparison between MFM and SXRMS on the same sample area. Here we combine both methods: the illuminated area on an $8 \mu\text{m}$ FePd wire is confined in the wire direction using a micro-scale pinhole.

The FePd wire preparation consisted of two steps: a pattern was defined using UV lithography on a silicon resist and the FePd layer was then Ar^+ ion etched down to the MgO substrate. The SXRMS measurements were performed using an in-vacuum diffractometer,¹² equipped with a charge-coupled device (CCD) camera, on beamline ID08 at the ESRF. The 16-bit Princeton Instruments CCD camera contains 1242×1152 square pixels, with a size s_{pxl} of $22.5 \mu\text{m}$. At low counting rates, individual x rays in the image could be easily observed as small spots with the size of a single pixel. The characteristics of the CCD were confirmed to fulfil the requirements for single-photon-counting detection.¹³ The CCD camera was fixed at an angle of $2\theta_i = 45^\circ$ at a distance d of 0.46 m from the wire sample, which was placed in

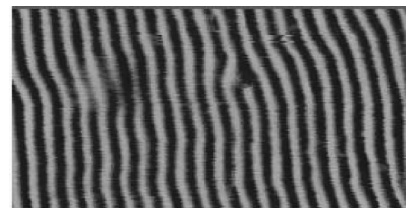


FIG. 1. MFM image of the magnetic stripe domains in FePd alloy, with a scale of $1 \times 2 \mu\text{m}^2$. The domains show up in dark and light shading corresponding to up and down magnetization, with a period of ~ 100 nm.

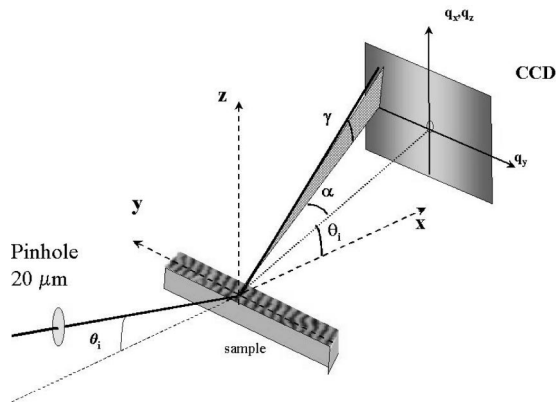


FIG. 2. Schematic layout of the scattering geometry in reflection using a CCD detector.

reflection geometry at an incidence angle of θ_i (cf. Fig. 2). To enhance the magnetic contrast the sample was illuminated with 100% circularly polarized soft x rays with the energy tuned to the Fe L_3 resonance. The vertical and horizontal rms source sizes of the APPLE II undulator is $\sigma_v \approx 10 \mu\text{m}$ and $\sigma_h \approx 400 \mu\text{m}$, respectively. The beamline includes horizontal focusing, a grating monochromator, and vertical focusing optics.

The longitudinal coherence length Λ_l is determined by the resolving power $\lambda/\Delta\lambda$ of the monochromator.¹⁴ At the resonance wavelength $\lambda = 1.75 \text{ nm}$ (700 eV), $\lambda/\Delta\lambda \approx 3000$, so that $\Lambda_l = \lambda^2/\Delta\lambda \approx 6 \mu\text{m}$. Given that the absorption length μ^{-1} in pure Fe at the L_3 edge is $\sim 30 \text{ nm}$,¹⁵ we might expect that for FePd in specular reflection the longitudinal coherence condition

$$\Lambda_l \gg \mu^{-1} \sin^2 \theta_i \tag{1}$$

is largely fulfilled at the resonance. A more general condition is required for the off-specular scattering employed here, but with small deviation from the specular case.

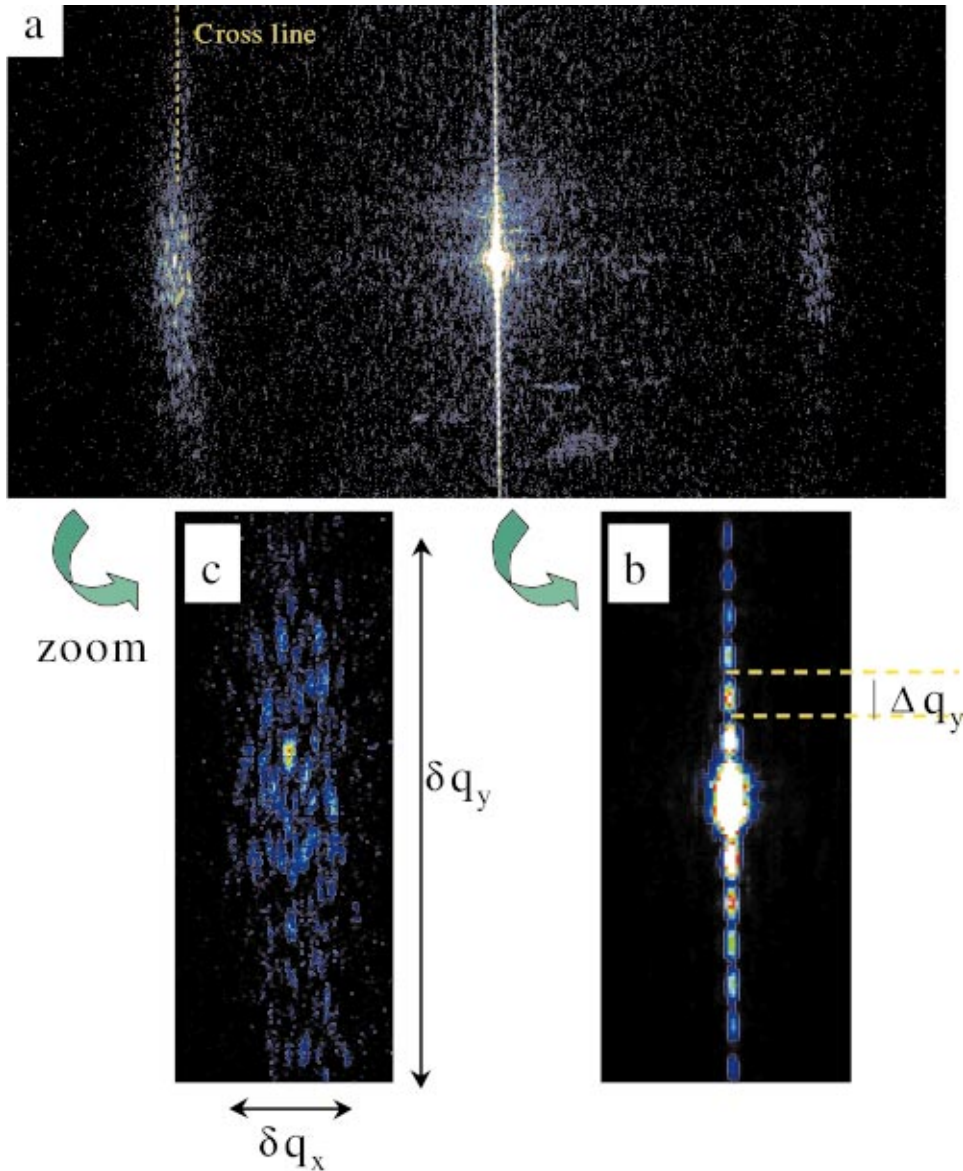


FIG. 3. (Color) (a) CCD x-ray image of 1237×594 pixels, corresponding to an accumulation of 200 exposures of 10 s. (b) Enlarged image of the oscillating streak along the vertical rod, which period in k space corresponds to the width of the wire ($8 \mu\text{m}$). (c) Enlarged image of magnetic speckles in the left magnetic satellite.

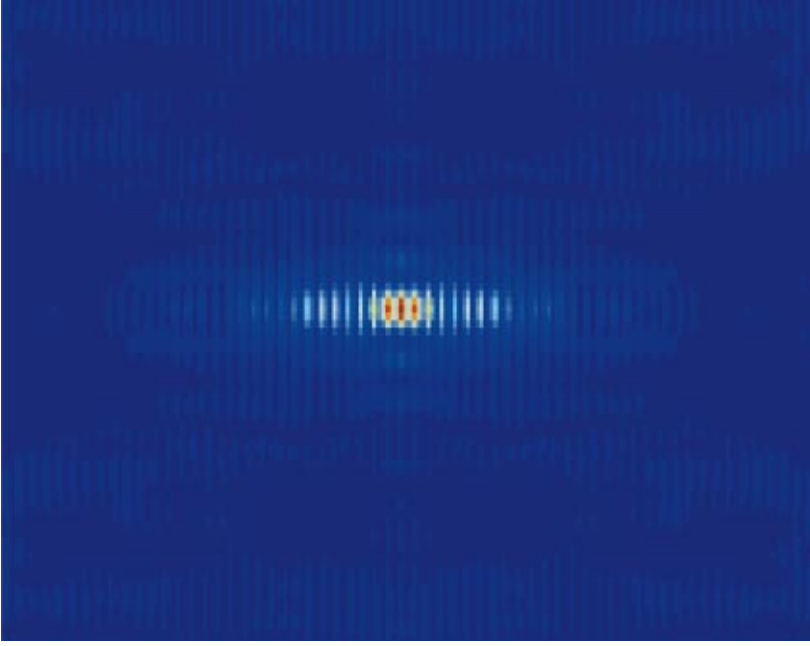


FIG. 4. (Color) Fourier transform of the image in Fig. 3(c) corresponding to the 2D magnetic correlation function. Vertical stripes are observed with a correlation length of ~ 20 periods of 100 nm.

Since $\sigma_h > \sigma_v$, the smallest transverse coherence length Λ_h is given by¹⁶

$$\Lambda_h \approx \frac{\lambda D}{\pi \sqrt{2} \sigma_h} \approx 58 \text{ } \mu\text{m} \quad (2)$$

for an overall beamline length $D = 58$ m. A circular pinhole of $\phi = 20 \text{ } \mu\text{m}$ was used, and to avoid plane-wave distortion, the sample should be in the near field of the pinhole. In our experimental setup the distance to the sample was $l = 50$ mm, which is small compared to the near-field limit of $\phi^2/\lambda \approx 230$ mm. The beam size ρ at the sample is then $\sqrt{\phi^2 + (1.22\lambda l/\phi)^2} \approx 20.7 \text{ } \mu\text{m}$, so that $\rho \approx \phi$.

For phase retrieval, the oversampling condition must be fulfilled,

$$s_{\text{pxl}} < \frac{1.22\lambda d}{s_y}, \quad (3)$$

$$s_{\text{pxl}} < \frac{1.22\lambda d}{s_x \sin \theta_i}, \quad (4)$$

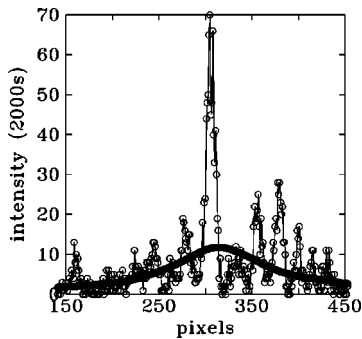


FIG. 5. Profile of the number of x rays observed along a vertical line across the magnetic satellite peak indicated in Fig. 3(c). The smoothed curve represents the calculated incoherent scattering.

where s_x and s_y give the size of the illuminated wire sample in the x and y directions (cf. Fig. 2). With the FePd wire perpendicular to the scattering plane, $s_y = 20 \text{ } \mu\text{m}$ and $s_x = 8 \text{ } \mu\text{m}$, thus satisfying the oversampling condition by a factor of 2 in the horizontal direction and a factor of 14 in the vertical one. Moreover, this geometry will explain the elongated shape of the spots in the recorded image.

The droplet algorithm¹³ was used to estimate the total number of photons in the detector. After each exposure the true x rays were extracted and the final image was obtained using accumulation. This method avoids pixel saturation and suppresses the electronic noise. The photon-counting mode also allows us to discriminate between speckle contrast and Poisson statistics. Figure 3(a) shows an image obtained from an accumulation of 200 exposures of 10 s, which amounts to a total of 33 min. We emphasize here the unprecedented quality of the picture: the high contrast results from the good coherent conditions and the unique stability of the ID08 beamline. This image exhibits a very intense central streak due to the specular reflection. On each side there is a magnetic satellite of significantly weaker intensity than the specular peak and appearing only when the energy is tuned at the resonance edge. While the specular maximum contains 10^5 photons/pixel, there are only ~ 100 and ~ 20 photons/pixel in the maximum of the left and right magnetic peaks, respectively. Note that some individual photons are present in the low-intensity regions, demonstrating the large dynamical range of the detection method.

In the reflection geometry the components of the scattering vector \mathbf{q} are given by

$$q_x \approx k \sin \theta_i \sin \gamma,$$

$$q_y = k \sin \alpha,$$

$$q_z \approx 2k \sin \theta_i, \quad (5)$$

where $k = 2\pi/\lambda$ is the wave vector of the incident beam. The angles α and γ , visualized in Fig. 2, determine the relative position on the CCD image with respect to the specular spot, defined by $\theta_i = 22.5^\circ$. Since α and $\gamma \leq 1.5^\circ$, q_z is almost constant while q_x and q_y are practically proportional to γ and α , respectively.

The central spot in Fig. 3(b) consists of a vertical rod with a modulation arising from diffraction at the wire edges. The sharp oscillations observed in this rod confirms that the wire has abrupt edges. The oscillation period (Δq_x) corresponds to a real-space width of $8 \pm 0.1 \mu\text{m}$, in agreement with the width of the wire as it was prepared. The elongated shape of the magnetic satellites arises partly from the reflection geometry which stretches the image in the vertical direction. The magnetic satellite position in k space corresponds to a transversal periodicity of the stripes of $95 \pm 2 \text{ nm}$ in real space, in agreement with the MFM results. The horizontal width δq_y of the satellite provides a way to estimate the periodicity fluctuation. This gives a transversal magnetic correlation length $l_{c,y} = 2\pi/\delta q_y \approx 2 \mu\text{m} \approx 20$ periods. The vertical extension δq_x of the satellites provides an estimate of the longitudinal correlation length along the stripes. This gives $l_{c,x} = 2\pi/\delta q_x \approx 700 \text{ nm}$, which is the average distance between defects, forks, and meandering in the stripes. Figure 4 shows the Fourier transform of the image, in which the 20-period correlation is apparent.

Figure 3(a) shows that the left magnetic satellite is more intense than the right one. Upon reversal of the light helicity the intensities of the satellites are interchanged. This dichroism in the transverse geometry evidences the presence of closure domains at the surface, which leads to an interference in the scattering between the amplitudes from the perpendicular and the in-plane magnetized domains. This effect was previously observed on FePd continuous films using a photodiode as detector,^{17,18} but here we show that it is also present in a single microwire.

The enlarged image in Fig. 3(c) shows the intensity fluctuations in the magnetic satellite. Although the counting statistics is low, the image displays a high speckle contrast, as expected from the coherence conditions. Due to the wire shape, the speckle size is largest in the vertical direction. Figure 5 shows the intensity profile $I(\mathbf{q})$ along a vertical line across the magnetic satellite image on the detector. Also plotted is the result of a two-dimensional smoothed intensity

$I_{inc}(\mathbf{q})$, which corresponds to the intensity profile observed using an incoherent beam. The overall degree of coherence β can be estimated from

$$\beta = \frac{\langle [I(\mathbf{q}) - I_{inc}(\mathbf{q})]^2 - I_{inc}(\mathbf{q}) \rangle}{\langle I_{inc}(\mathbf{q})^2 \rangle}, \quad (6)$$

which is a ratio between the intensity square variations, corrected from the Poisson contribution, and the square of the smoothed intensity. The brackets $\langle \dots \rangle$ mean an average over the area corresponding to the magnetic satellites. From this we obtain $\beta = 0.85 \pm 0.05$. Such a high degree of coherence creates excellent conditions for the reconstruction of the magnetic disorder in real space. The last requirement deals with the spatial resolution. In practice, the reconstruction algorithms are expected to converge when the pinhole illuminates at most a few hundreds objects, which is the case here: ~ 400 magnetic stripes. In the present setup, the CCD dimensions limit the ultimate spatial resolutions d_x and d_y for the sample:

$$d_x = \frac{1}{q_{x,\text{max}}} \approx \frac{\lambda}{2\pi\gamma_{\text{max}}\sin\theta_i} \approx 50 \text{ nm},$$

$$d_y = \frac{1}{q_{y,\text{max}}} \approx \frac{\lambda}{2\pi\alpha_{\text{max}}} \approx 10 \text{ nm}. \quad (7)$$

Since the magnetic period is 100 nm, the spatial resolution d_y is sufficient to access the morphology in real space.

In summary, soft-x-ray magnetic speckles in reflection geometry have been observed using two-dimensional imaging. The presence of magnetic speckles, displaying a very high magnetic contrast, has been proven unambiguously. The large oversampling of our experiment gives some information for evaluating the scattering amplitude phase and for real space reconstruction. Our work opens up the possibility to use SXRMS for the study of static and dynamic magnetic disorder on length scales relevant for nanomagnetism. This photon-in–photon-out technique allows us to study reversal processes as a function of magnetic field and temperature as well as ultrashort dynamical behavior.

ACKNOWLEDGMENTS

We thank M. D. Roper, A. Haznar, C. Teodorescu, G. Guénot, and N. B. Brookes for their expert assistance during the experiments. We are grateful to J. L. Thomassin and H. Sibuet for their help in preparing the samples.

*Email address: chesnel@drfmc.ceng.cea.fr

†Email address: flivet@ltpcm.inpg.fr

‡Email address: g.vanderlaan@dl.ac.uk

¹J.M. Tonnerre *et al.*, Phys. Rev. Lett. **75**, 740 (1995).

²M. Sacchi *et al.*, Phys. Rev. Lett. **81**, 1521 (1998).

³G. van der Laan, Synchrotron Radiat. News **14**(5), 32 (2001).

⁴A.C. Price *et al.*, Phys. Rev. Lett. **82**, 755 (1999).

⁵S. Brauer *et al.*, Phys. Rev. Lett. **74**, 2010 (1995).

⁶F. Livet *et al.*, Phys. Rev. E **63**, 036108 (2001).

⁷Z.H. Cai *et al.*, Phys. Rev. Lett. **73**, 82 (1994).

⁸J.F. Peters *et al.*, ESRF Newsletter **32**, 12 (2000).

⁹B. Hu *et al.*, Synchrotron Radiat. News **14**(2), 17 (2001).

¹⁰V. Gehanno *et al.*, Phys. Rev. B **55**, 12 552 (1997).

¹¹P. Kamp *et al.*, Phys. Rev. B **59**, 1105 (1999).

¹²G. van der Laan *et al.*, Synchrotron Radiat. News **12**(3), 5 (1999).

¹³F. Livet *et al.*, Nucl. Instrum. Methods Phys. Res. A **451**, 596 (2000).

¹⁴See e.g., L. Mandel and E. Wolf, *Optical Coherence and Quantum Optics* (Cambridge University Press, Cambridge, England, 1995), p. 149.

¹⁵R. Nakajima, J. Stöhr, and Y.U. Idzerda, Phys. Rev. B **59**, 6421 (1999).

¹⁶See, e.g., Ref. 14, p. 286.

¹⁷H.A. Dürr *et al.*, Science **284**, 2166 (1999).

¹⁸E. Dudzik *et al.*, Phys. Rev. B **62**, 5779 (2000).